Mastering the structure of PLA foams made with extrusion assisted by supercritical CO2

Margot Chauvet, Martial Sauceau, Fabien Baillon, Jacques Fages

HAL Id: hal-01619251
https://hal.science/hal-01619251

Mastering the structure of PLA foams made with extrusion assisted by supercritical CO₂

Margot Chauvet, Martial Sauceau, Fabien Baillon, Jacques Fages
Centre RAPSODEE, Université de Toulouse; Ecole des Mines d'Albi, CNRS, Albi F-81013, France
Correspondence to: J. Fages (E-mail: Jacques.Fages@mines-albi.fr)

INTRODUCTION

Foams of poly(lactic acid) (PLA) are of great interest due to the specific properties of this polymer. It is derived from lactic acid, which can be obtained by fermentation from renewable agricultural sources like corn starch.[1] It is therefore a biobased polymer and it presents comparable mechanical properties as those of polystyrene (PS). PLA could replace PS foams in cushioning, insulation or construction applications.[2] This polymer is also biodegradable, it is degraded primarily by hydrolysis, after several months of exposure to moisture.[1] Foaming PLA, could be particularly interesting for packaging applications, especially the disposable packaging foams. These products are usually made from expanded polystyrene (EPS). Despite of the excellent properties of EPS (low density, low cost, and strength), some concerns are raised by the impact of the manufacturing process and the disposal in the environment.[3] PLA foams could address this issue. Moreover, PLA presents biocompatible and bioresorbable properties in the human body. It will not induce any sustained inflammatory or toxic response upon implantation.[4] PLA foams could be used to manufacture three dimensional structures used for cell attachment and tissue regeneration, the so called tissue engineering scaffolds.[5,6]

Usually, foams are made using a chemical blowing agent (CBA)[7] or by injection of a physical blowing agent (PBA) in the molten polymer. Because CBAs leave residues in the polymer phase and most of PBAs exhibit deleterious effects like the depletion of the ozone layer as well as some hazardous properties, their replacement is highly recommended.[8] Supercritical carbon dioxide (sc CO₂) is the most favorable replacement candidate due to its unique properties, such as environmental friendliness, non flammability, and low cost. Its inert nature, and mild critical conditions [critical temperature (T_c) of 31 °C and critical pressure (P_c) of 7.38 MPa] are additional advantages. Moreover, CO₂ is well known for its good compatibility with several polymers in which its solubility can be relatively high depending however on the temperature and pressure conditions. In the process of extrusion assisted by sc CO₂, the supercritical fluid will change the rheological properties of the material inside the extruder and will play the role of an expansion agent at the die exit.[9]

Several studies of the literature have described the extrusion foaming of PLA with sc CO₂[10–23] and have been reviewed in recent publications.[2,24,25] In most of these studies, the relationship between die temperature and porosity has been investigated. It has been shown that with decreasing die temperature, porosity and expansion ratio increased.[13,14,16,17,20,22,23] The effect of sc CO₂ content on the foam density has been mainly investigated.[10,13] It has been shown that the CO₂ content has to be above 7 wt % for giving highly expanded foams. Pilla et al.,[14] Mihai et al.,[15] and Wang et al.[16] demonstrated that adding a chain extender (CE) to PLA helps increasing the expansion ratio due to an improvement of the melt strength. The
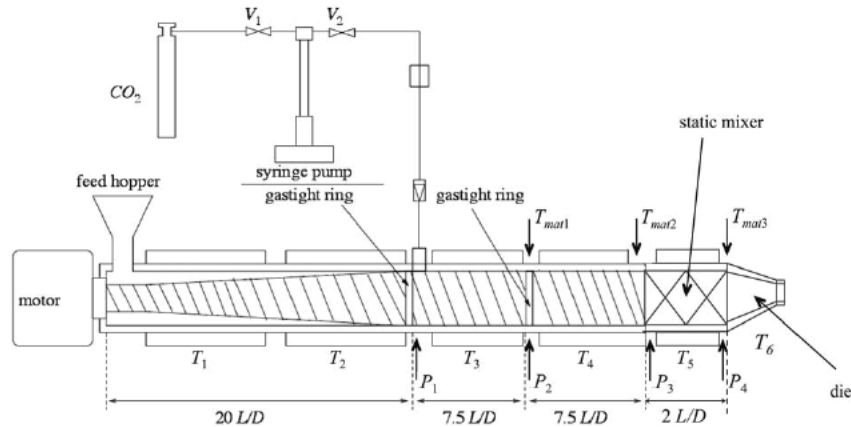
Figure 1. Experimental device.

addition of a nucleating agent, such as talc or clay, will lead to a finer cell structure and higher cell density.[10,14] Keshtkar et al.,[17] Matuana and Diaz,[18] and Jiang et al.[19] found an increased cell density, expansion ratio, and melt strength, following nanoclay addition as a cell nucleation agent. Nofar[22] showed that well dispersed nanoparticles (micro sized talc, nanosilica, and nanoclay) enhanced the expansion ratio and cell density of the foamed samples, thanks to a large number of induced crystals through the nanoparticles. Extrusion foaming of PLA has also been implemented in blend with poly(butylene adipate co terephthalate) (PBAT),[20] another biodegradable polymer, or with natural fibres,[23] and the effect of temperature on final properties has been studied. In the case of wood flour addition,[21] authors have observed the effect of the melt flow index (MFI) on the foam properties.

Despite numerous reports on PLA foaming, the importance of operating conditions on the foam morphology and expansion at the end of the die has not yet been studied extensively. Park et al.,[26] Lee et al.,[27] and Huang et al.[28] showed with LDPE/PS or polycarbonate polymers that there was an optimal die temperature for maximizing the open cell content. Naguib et al.[29] highlighted the relation between gas loss, crystallization, and radial expansion with polypropylene foams.

In this study, we have chosen to focus on two process parameters, die temperature and CO_2 content, and their effect on PLA foams characteristics. The porosity, the type of expansion, the morphology and the crystallinity of the foams will be investigated.

EXPERIMENTAL

Materials

The poly(lactic acid) used is a semicrystalline grade (PLE001, NaturePlast) with a MFI about 6 g 10 min^{-1} (210 °C, 2.16 kg). Its density, measured by water pycnometry, is equal to 1230.9 kg m^{-3}. DSC cycle has shown a glass transition at 59 °C and the melting temperature is approximately 150 °C.

Carbon dioxide (CO_2) with a purity of 99.995%, supplied by Air Liquide, was used as PBA.

Extrusion Foaming

The experimental set up has previously been detailed elsewhere[30-33] and is shown in Figure 1. The single screw extruder has a 30 mm screw diameter and a length to diameter ratio (L/D) of 37 (Rheoscam, SCAMEX). It is divided into four parts. The three first parts correspond to the screw of length 1.05 m. The length to diameter ratio is 20 for the first zone, and 7.5 for the two following zones. Additional part of 2 L/D, corresponding to a static mixer, is added at the end of the extruder. Between each part, a restriction ring has been fitted out in order to obtain a dynamic gastight, which prevents sc CO_2 from back flowing. The first part with a tapered channel between the threads allows the transport of solid polymer pellets and then, their melting and plasticizing. In the two following parts, the screw has a cylindrical geometry and a constant channel depth from the first gastight ring to the end. The fourth part, which is removable, contains four static mixer elements with a diameter of 17 mm (SMB H 17/4, Sulzer). In this work, a cylindrical die of 3 mm diameter and 12 mm length was used. The temperature inside the barrel is regulated at six locations: T_1 and T_2 before the CO_2 injection, T_3 and T_4 after the injection, T_5 in the static mixer, and T_6 in the die.

There are four pressure and three temperature sensors: P_1 after the CO_2 injector, P_2 and T_{mat1} before the second gastight ring, P_3 and T_{mat2} before the static mixer and P_4 and T_{mat3} by the die.

Table I. Operating Conditions

	Operating conditions
N	30 rpm
T_1	160 °C
T_2	180 °C
T_3	180 °C
T_4	160 °C
T_5	100–160 °C
T_6	T_5
$\dot{V}_{CO_2}$	1.5–3.5 mL min^{-1}

Table II. Samples Collected

Sample name	T_6 (°C)	$\dot{V}_{CO_2}$ (mL min^{-1})	$\dot{m}^m_{polymer}$ (g min^{-1})	P_1 (MPa)	$\rho^{pump}_{CO_2}$ (g mL^{-1})	w_{CO_2} (%)
160 0	160	0	43.8	15.2	0.9792	0
154 0	154	0	45.6	15.8	0.9818	0
150 0	150	0	44.1	15.9	0.9823	0
144 0	144	0	43.2	17.0	0.9870	0
140 0	140	0	42.9	17.3	0.9883	0
132 1.5	132	1.5	42.2	17.7	0.9901	3.4
129 2	129	2	41.7	18.7	0.9944	4.5
125 2	125	2	41.3	18.6	0.9940	4.6
120 2	120	2	40.5	19.4	0.9975	4.7
115 2	115	2	41.0	19.8	0.9992	4.6
115 2.5	115	2.5	40.4	19.5	0.9979	5.8
112 2.5	112	2.5	40.0	19.7	0.9988	5.9
111 3	111	3	44.2	20.1	1.0005	6.4
109 3.5	109	3.5	39.0	22.4	1.0105	8.3
108 3.5	108	3.5	38.5	21.5	1.0066	8.4
107 3	107	3	40.0	21.2	1.0053	7.0
105 3	105	3	38.6	21.8	1.0079	7.3
103 3.5	103	3.5	37.9	23.6	1.0157	8.6
102 3.5	102	3.5	39.0	23.8	1.0166	8.4

CO_2 is pumped from a cylinder by a syringe pump (260 D, ISCO). The pressure in the CO_2 pump is kept slightly higher than the pressure P_1. The CO_2 injector is positioned at a length to diameter ratio of 20 from the feed hopper. It corresponds to the beginning of the metering zone, i.e., the part where the channel depth is constant and equal to 1.5 mm.

Some operating conditions were kept constant, such as the screw speed N and the temperature from T_1 to T_4, while T_5, T_6, and CO_2 flow rate ($\dot{V}_{CO_2}$) have been varied. They are listed in Table I. In this study, T_2 and T_3 were fixed at 180 °C to ensure a molten polymer in the barrel before and after the CO_2 injection.[13] T_5 and T_6 were first set up at 160 °C before injecting the CO_2. Then, T_5 and T_6 were lowered together to get a high enough pressure inside the extruder. The foaming experiments began with T_5 and T_6 fixed at 140 °C and a constant $\dot{V}_{CO_2}$ of 1.5 mL min^{-1}. Then, step by step, the temperature in the static mixer (T_5) and in the die (T_6) were lowered together ($T_5 = T_6$) and samples collected on a period of 30 s once the system has reached a steady state. Lowering T_5 and T_6 may lead to raise the torque and eventually to stop the engine due to safety cut off. Therefore, there is a need for an enhanced plasticization to diminish viscosity and consequently the torque and pressure P_4. This could be obtained by an increase in $\dot{V}_{CO_2}$, carbon dioxide being more soluble at lower temperatures. The experiments were stopped when the syringe pump was empty.

The samples collected are named $T\ \dot{V}_{CO_2}$ with T the temperature T_6 and $\dot{V}_{CO_2}$ the CO_2 flow rate. For example, the sample 111 3 was made at 111 °C with 3 mL min^{-1} of CO_2. Table II inventories the samples collected during the trials of extrusion foaming. $\dot{m}^m_{polymer}$ is the mass flow rate of polymer measured at

the die exit [calculated with eq. (1)], by collecting and weighing a sample of mass m on a period t of 30 s.

$$\dot{m}^m_{polymer} = \frac{m}{t} \tag{1}$$

With the polymer mass flow rate and the CO_2 flow rate, the mass fraction of CO_2 (w_{CO_2}) can be calculated with eq. (2)

$$w_{CO_2} = \frac{\dot{V}_{CO_2}\rho^{pump}_{CO_2}}{\dot{V}_{CO_2}\rho^{pump}_{CO_2} + \dot{m}^m_{polymer}} \tag{2}$$

$\rho^{pump}_{CO_2}$ is the CO_2 density at 5 °C (pump temperature) and at P_1, the pressure in the injection port (listed in Table II), obtained on NIST website and calculated by the Span and Wagner equation of state.[34,35]

Foam Characterizations

Porosity. The foam porosity (ε_T), representing the ratio of void volume to the total volume of the sample, can be calculated by eq. (3)
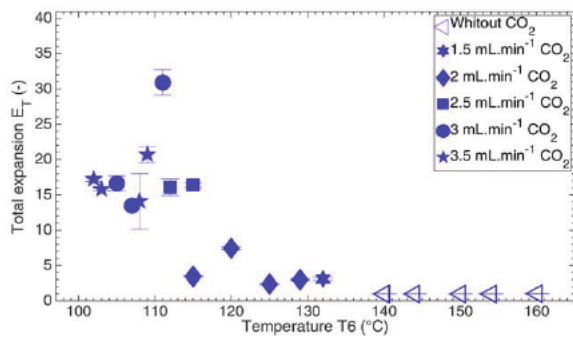
$$\varepsilon_T = \frac{V_{Total\ porosity}}{V_{Total}} = 1 - \frac{\rho^{H_2O}_f}{\rho^{H_2O}_p} \tag{3}$$

With $\rho^{H_2O}_f$ the apparent density of the foamed sample, determined by water pycnometry and ρ^{H2O}_p the solid polymer density, determined by water pycnometry (AccuPYC 1330, Micromeretics).

The open porosity (ε_O), representing the ratio of open cell to the total volume of the sample can be calculated by eq. (4)
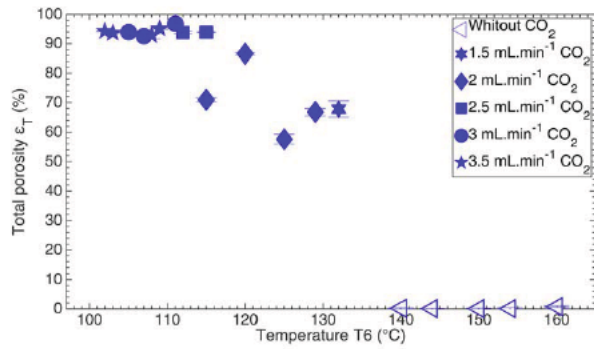
a) Total porosity as a function of temperature T_6

b) Total expansion as a function of temperature T_6

Figure 2. Total porosity and expansion as a function of temperature T_6. [Color figure can be viewed at wileyonlinelibrary.com]

$$\varepsilon_O = \frac{V_{Open\ porosity}}{V_{Total}} = 1 \quad \frac{\rho_f^{H_2O}}{\rho_f^{He}} \tag{4}$$

With ρ_f^{He}, the density of the foamed sample excluding open pores determined by helium pycnometry.

The open cell content (OC), representing the ratio of open porosity to the total porosity, can be calculated by eq. (5)

$$OC = \frac{\varepsilon_O}{\varepsilon_T} \tag{5}$$

Thermal Analysis. Modulated differential scanning calorimetry (MDSC, Q2000, TA Instruments) was performed to evaluate the thermal properties and the crystallinity of the foams. Three signals are given by MDSC:

- Total heat flow (THF) (same as usual DSC)
- Reversing heat flow (revHF) (linked to the heat capacity, C_p)
- Nonreversing heat flow (nonrevHF) (linked to the heating kinetics)

Glass transition of the sample will be deduced from the revHF signal. NonrevHF shows the crystallization while THF shows the melting.

The analyses were performed on Heat Only mode, from 10 to 200 °C with a heating ramp of 2 °C min ^{1}. An amplitude of 0.32 °C will be applied with a time period of 60 s.

The crystalline content of the sample is calculated as follows:

$$\chi = \frac{\Delta H_m \quad \Delta H_{cc}}{\Delta H_{m\infty}} \tag{6}$$

with ΔH_m the melting enthalpy, ΔH_{cc} the cold crystallization enthalpy, and $\Delta H_{m\infty}$ the heat of fusion of PLA for a perfect crystal, known to be 93 J g ^{1}.[36]

X ray Diffraction. Samples were first compressed in disk shape using an Instron press. Wide angle X ray diffraction (WXRD) patterns of foamed PLA were then obtained with an X ray diffractometer (X'Pert PRO MPD, PANalytical). The samples were exposed to an X ray beam generated by a tube with a copper anticathode. The diffraction patterns were collected over an angular range (2θ) between 5.5° and 45.0° with an incremental step of 0.033° and a time of acquisition of 139.7 s dot ^{1}.

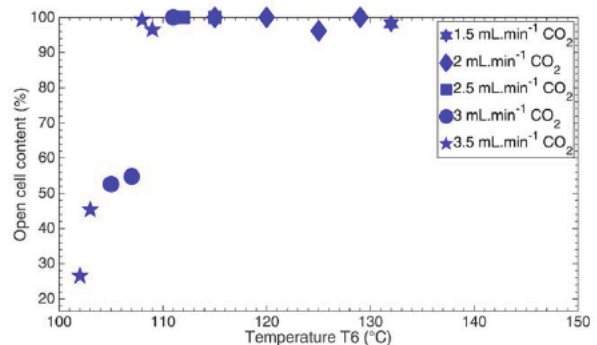**Expansion.** The total expansion (E_T) can be expressed on the basis of the porosity with eq. (7)

$$E_T = \frac{\rho_p^{H_2O}}{\rho_f^{H_2O}} = \frac{1}{1 \quad \varepsilon_T} \tag{7}$$

The total expansion provides the same type of information as porosity but with a special emphasis on high porosity range.

Depending on the CO_2 content, the maximum expansion ratio (E_T^M) can be calculated with eq. (8)[37]
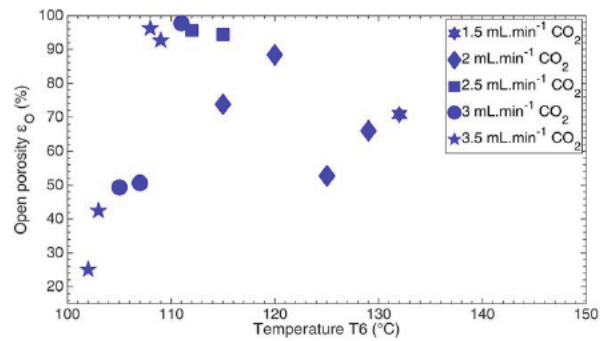
a) Open porosity as a function of temperature

b) Open cell content as a function of temperature

Figure 3. Open porosity and open cell content of the foams in function of temperature. [Color figure can be viewed at wileyonlinelibrary.com]
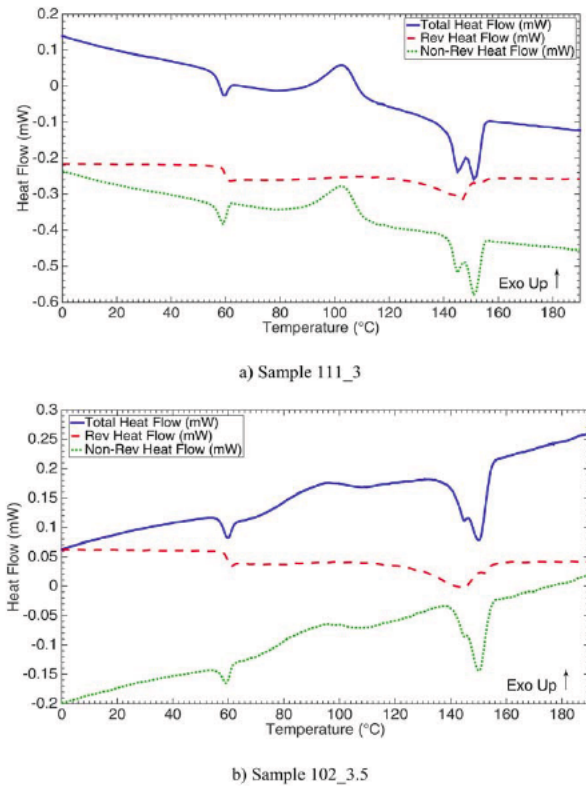
a) Sample 111_3

b) Sample 102_3.5

Figure 4. MDSC cycle. (a) Sample made at 111°C and 3 mL min^{-1} of CO_2, (b) sample made at 102°C and 3.5 mL min^{-1} of CO_2. [Color figure can be viewed at wileyonlinelibrary.com]

$$E_T^M = \frac{V_{polymer} + V_{CO_2}^{amb}}{V_{polymer}} = 1 + \frac{w_{CO_2}}{1 - w_{CO_2}} \times \frac{\rho_p^{H_2O}}{\rho_{CO_2}^{amb}} \qquad (8)$$

with w_{CO_2} the mass fraction of CO_2, $\rho_p^{H_2O}$ the solid polymer density, and $\rho_{CO_2}^{amb}$ the CO_2 density at room pressure and temperature being 1.78×10^{-3} g cm^{-3} (Nist table[34]). This calculation is made with the assumption of no CO_2 escape from the sample.[16]

The ratio of expansion (R_E) is the total expansion ratio (E_T) divided by the maximal theoretical expansion ratio (E_T^M). This ratio of expansion gives information about the exact quantity of CO_2 used to expand the foams.

The radial expansion (E_R) was calculated by dividing the diameter of the sample measured with a caliper (average of 10 measurements) by the die diameter (3 mm).

The longitudinal expansion (E_L) was quantified by measuring the sample length exiting the extruder in a period of 30 s with and without CO_2, E_L being the ratio of the two. The main contribution to the volumetric throughput comes from the screw rotation speed, independently of the melt polymer properties.[38] Therefore, the assumption of a constant volumetric throughput before the die was made, whatever the operating conditions. In consequence, the increase of the matter velocity at the die exit was considered as representative of the longitudinal gas expansion. The speed of the unfoamed sample, 2.8 m min^{-1} for a screw rotation of 30 rpm at 160°C, was taken as a reference for all calculations.

Mass Balance. As previously explained, the measured mass flow rate $\dot{m}_{polymer}^m$ is obtained by collecting samples on a period t of 30 s. Knowing the dimensions, diameter d, length L, and the apparent density of the foamed sample, a mass flow rate could be calculated with eq. (9)

$$\dot{m}_{polymer}^c = \rho_f^{H_2O} \frac{d^2 L \pi}{4t} \qquad (9)$$

The measured and calculated values of the mass flow rate could then be compared.

Morphology. The samples were observed by environmental scanning electron microscopy (ESEM, FEG, Philips). Back scattered electrons (BSE) mode was used with a potential of 25 kV. Pictures were taken on cross sections perpendicular to the flow, obtained by fracturing the sample by hand.

RESULTS AND DISCUSSION

Porosity

Plot of total porosity as a function of temperature is shown in Figure 2(a). For samples without CO_2, there is almost no porosity (less than 0.7%). The addition of CO_2 in the extruder, even in very small quantities, creates porosity. With only 1.5 mL min^{-1} of CO_2 (i.e., 3.4 wt % in the polymer), a porosity over 60% is created.

Gas escape must be prevented to obtain high porosity.[37] This can be achieved by freezing the "skin" of the extrudate with a low die temperature. Moreover, the polymer melt should be

Table III. Parameters Determined by the MDSC

| Samples | Reversible HF | | Nonreversible HF | | Total HF | | |
	T_g (°C)	ΔC_p (J g^{-1} °C^{-1})	T_{cc} (°C)	ΔH_{cc} (J g^{-1})	T_m (°C)	ΔH_m (J g^{-1})	χ (%)
160 0	59.8	0.4	97.0	30.1	142.9	30.3	0.2
140 0	60.7	0.5	92.3	22.9	141.2	25.3	2.6
111 3	59.8	0.6	88.3	19.9	141.2	25.9	6.4
108 3.5	59.6	0.5	91.5	21.6	140.8	25.9	4.6
105 3	59.4	0.4	72.7	14.7	140.6	24.6	10.7
103 3.5	59.6	0.4	76.3	13.1	139.7	27.4	15.3
102 3.5	59.8	0.4	77.6	12.1	139.5	25.7	14.6

Figure 5. XRD patterns of foamed PLA. [Color figure can be viewed at wileyonlinelibrary.com]

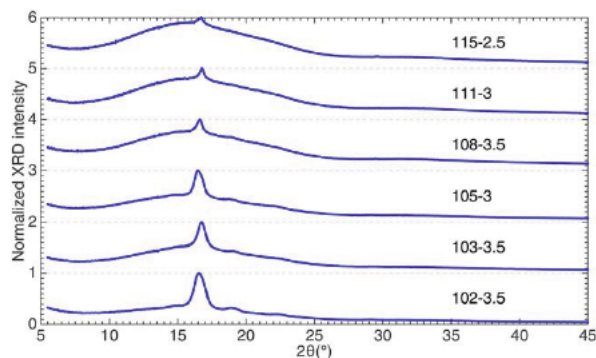**Figure 6.** Pressure P_4 as a function of temperature T_6. [Color figure can be viewed at wileyonlinelibrary.com]

cooled substantially upstream the die, to increase its strength in order to prevent cell coalescence and to insure a high cell density while keeping a sufficient fluidity for bubbles to grow.[39] With decreasing die temperature, the amount of gas loss will also decrease by the diffusivity diminution. As a result, a greater amount of gas will be retained in the foam, leading to a large total expansion.[40] Figure 2(a) shows that, by decreasing die temperature associated to a rise in CO_2 content, porosity as high as 96% could be obtained. The maximum porosity obtained was 96.8% at 111 °C with 6.4 wt % of CO_2 for sample 111 3.

Then, with further lowering die temperature, the porosity decreased slightly (from 96% to 93%), as shown in Figure 2(a) below a die temperature of 109 °C. This phenomenon of decreasing porosity (or total expansion) below a critical temperature has been described for PLA foams[16,17,19,20] and explained by an increasing stiffness of the polymer limiting the full expansion of the foams.

As explained in the Experimental section [see eq. (7)], the total expansion is directly linked to the porosity but gives a better vision of the effect especially at the higher values. As it can be seen in Figure 2(b), above 115 °C, the total expansion is very low (under 5). With the decrease of the die temperature and associated to a raise in CO_2 content, the total expansion increased until reaching a maximum of 30.9 before decreasing.

As it can be seen in both figures, at 115 °C, two different CO_2 contents were used. The more CO_2, the more porous the sample will be. This effect has already been reported by Lee *et al.*[27]

Figure 3(a) shows the open porosity as a function of temperature. In the high temperature range, the lower the temperature, the higher the open porosity. Then, below 107 °C, the open porosity decreased. Similar results were found by Lee *et al.*[27] with polycarbonate. Plotting the open cell content (ratio between the open porosity to the total porosity) as a function of temperature [Figure 3(b)] shows that above this critical temperature of 107 °C, the open cell content is 100%. Therefore, all porosity created is an open porosity. Then, below this critical temperature, both open and closed porosities are created.

In the high temperature range, with the decreasing temperature, diffusivity decreased, and thus, less gas can escape.[27] More gas
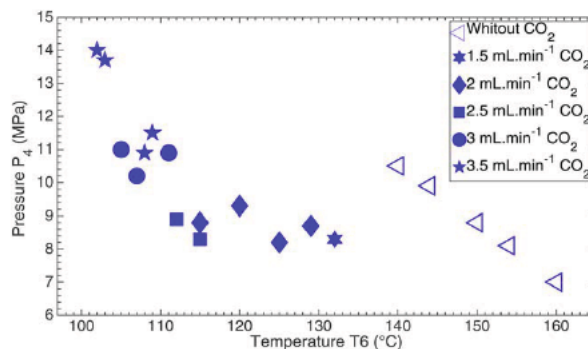
remaining in the foams, the porosity increased (Figure 2), but this goes with a diminution of the cell wall thickness, which were more easily opened.[27] With further decreasing temperature, melt strength increased and cell walls remain closed because of stiffness augmentation.

Thermal Analysis and Crystallization

Foams were analyzed by MDSC. Two curves are presented on Figure 4 and the values of all samples are listed in Table III. The glass transition temperature of all samples is about 59 °C, showing no effect of the foaming with sc CO_2. The glass transition is followed with an endothermic peak corresponding to an enthalpic relaxation due to ageing of the polymer.[41,42]

During the heating cycle, a crystallization peak appears as shown in Figure 4, which corresponds to the crystal formation. For samples made between 108 and 160 °C, as illustrated in Figure 4(a) for sample 111 3, the crystallization peak is large with an enthalpy of about 21 J g^{-1}. Besides, for samples made between 102 and 105 °C, the crystallization peak appears broader with an enthalpy of about 13 J g^{-1} [Figure 4(b) for sample 102 3.5]. For these three samples, this peak begins at lower temperature, indicating a change in crystallization kinetics.

After this exothermic peak, for samples made between 108 and 160 °C, two endothermic peaks, corresponding to the melting, are observable on the total heat flow [Figure 4(a)]. The double
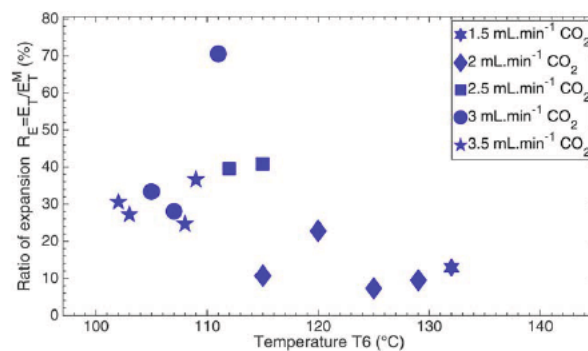

Figure 7. Ratio of expansion R_E as a function of temperature T_6. [Color figure can be viewed at wileyonlinelibrary.com]

a) Radial expansion as a function of temperature

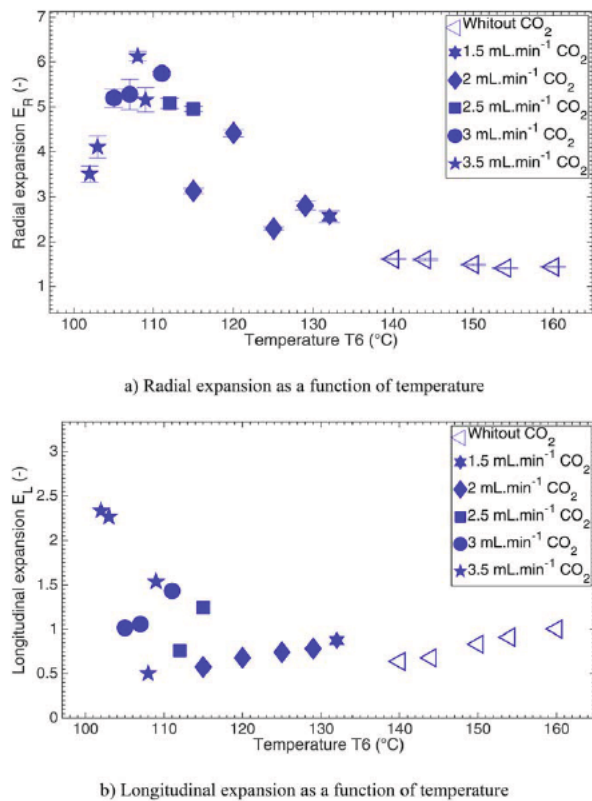
b) Longitudinal expansion as a function of temperature

Figure 8. Radial and longitudinal expansion of the foams in function of the temperature T_6. [Color figure can be viewed at wileyonlinelibrary. com]

melting behavior of PLA is already known and explained by the melt recrystallization model.[43] According to this model, the first peak is attributed to the melting of some amount of the original crystals while the second is ascribed to the melting of crystals formed through a melt recrystallization process during the heating. The exothermic peak between the double melting peaks is attributed to a recrystallization. Samples made between 102 and 105 °C show only one melting peak with a little shoulder [Figure 4(b)]. All samples present a melting enthalpy of approximately 25 J g $^{-1}$.

The crystallinity of the sample was calculated with eq. (6) (Table III). For temperatures higher than 108 °C, the crystallinity is low (around 5%), but below 105 °C, an increase of the crystallinity can be seen (15%). The increasing crystallinity is linked to the shear inside the extruder and to the CO_2 addition. At high temperature, thermal agitation prevails (due to the smaller characteristic times), and therefore, there is no effect of shear on the crystallinity because the polymer chains are arranged randomly. On the contrary, at low temperature, with shear and longer characteristic times of thermal agitation, molecules have more time to reorganise, facilitating the crystallization.[16] It is known that CO_2 has an effect on the crystallinity and crystallization rate of PLA.[44,45] Nofar et al.[44] have observed that the crystallization rate of PLA with low D lactide content was increased with addition of dissolved CO_2. They also

observed that crystallinity was affected by the density of nuclei on the molecular mobility of PLA and by the resultant plasticization effect of CO_2 at different CO_2 pressure. For Tsutsumi et al.,[45] DSC results have shown that the PLA crystallinity changes depend on temperature and pressure during CO_2 treatment. This is due to the rearrangements of the lamellar structures in the crystalline region. They conclude that the inclusion of CO_2 molecules affects the re arrangement of the polymer chains and hence the crystallinity.

PLA is known to have an inherently low melt strength[42] which does have an effect on expansion during the foaming process.[2] Improving the PLA crystallization can enhance the PLA melt strength by overcoming its weak viscoelastic properties and thereby improving its foamability.[2,12,13,16,46] Indeed, crystallization during foaming can improve PLA low melt strength through the network of nucleated crystals[12,15,16] and help producing low density foams by minimizing gas loss. Wang et al.[16] have highlighted the relation between crystallinity and melt strength. They have shown that the storage modulus has increased by 2 orders of magnitudes for a sample with 15% crystallinity, suggesting that crystallization has a major influence on melt strength.

In our case, samples made at low temperatures (102 105 °C) exhibit a rather large crystalline content as shown in Table III. It is assumed that this higher crystallinity compared to those of the other samples can lead to an increased polymer melt strength during the extrusion process. This is also in agreement with the porosity diminution under 109 °C shown on Figure 2 (93% for temperatures between 102 and 105 °C instead of 96% at 109 3.5) when the polymer melt strength becomes too high and limits the expansion.

In Figure 5, normalized XRD patterns of PLA foams made with different operating conditions are compared. All samples show a crystalline peak. With decreasing temperature, a much sharper peak can be seen, indicating a higher crystallinity. This is in good correlation with the MDSC results and the crystalline content listed in Table III. The peaks can be seen at $2\theta = 16.4°$ which correspond to α crystals.[47,48]

Figure 6 represents the die pressure P_4 as a function of die temperature. Below a threshold temperature close to 110 °C, even with an increase in the CO_2 content, the pressure inside the extruder increases greatly. Between 110 and 130 °C, the pressure stays constant at approximately 9 MPa. This is probably due to the compensation between two contradictory effects on viscosity: lower temperature and higher CO_2 content. But, under 110 °C, the pressure increases up to 16 MPa even at higher CO_2 contents, due to the predominant effect of temperature on viscosity. This seems to be associated with an increased melt strength as the porosity decreased (Figure 2) and the crystallinity increased (Table III).

Expansion

The ratio of expansion (R_E) is plotted versus the temperature T_6 in Figure 7. At low CO_2 content (1.5 and 2 mL min $^{-1}$, i.e., 3.4 and 4.7% of CO_2), the difference between E_T^M and E_T is large, leading to a small R_E of about 10%, indicating a large
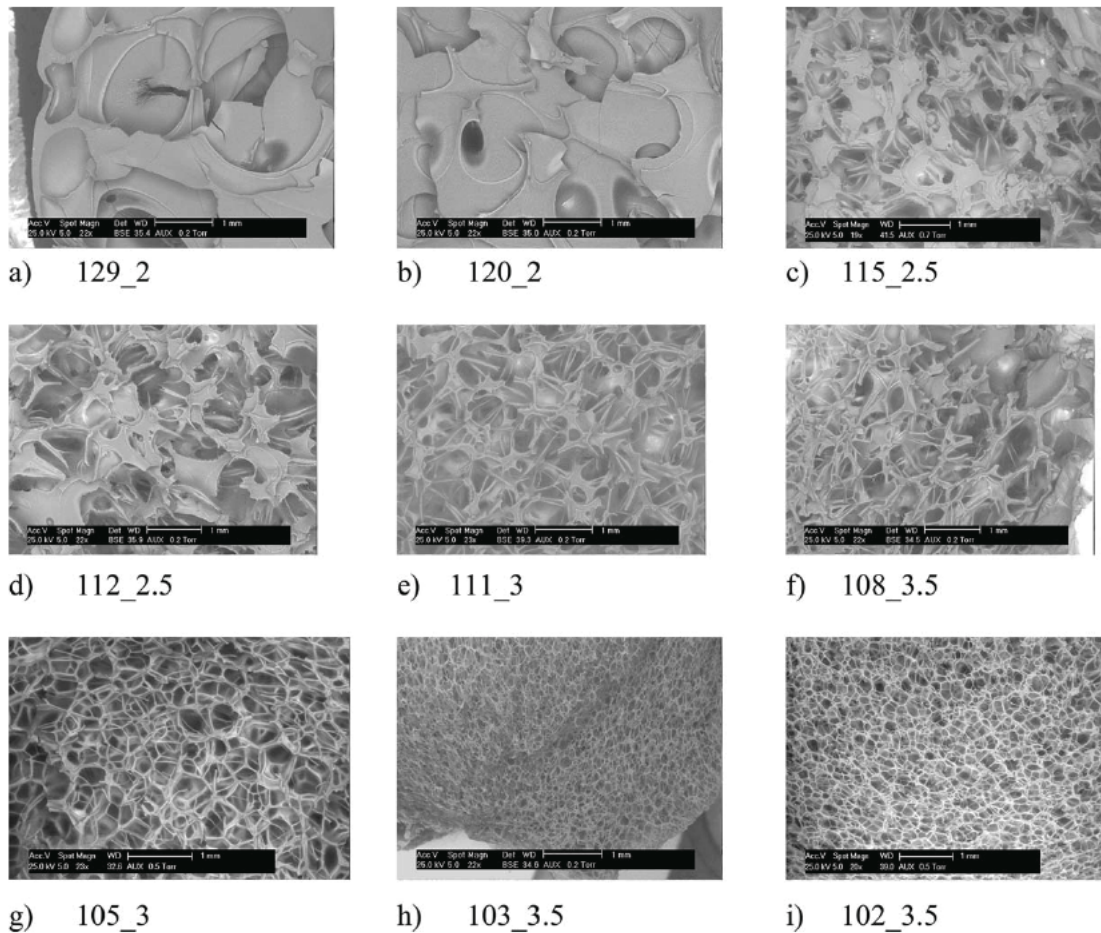
Figure 9. SEM images. (a) Sample made at 129 °C and 2 mL min⁻¹ CO_2, (b) sample made at 120 °C and 2 mL min⁻¹ CO_2, (c) sample made at 115 °C and 2.5 mL min⁻¹ CO_2, (d) sample made at 112 °C and 2.5 mL min⁻¹ CO_2, (e) sample made at 111 °C and 3 mL min⁻¹ CO_2, (f) sample made at 108 °C and 3.5 mL min⁻¹ CO_2, (g) sample made at 105 °C and 3 mL min⁻¹ CO_2, (h) sample made at 103 °C and 3.5 mL min⁻¹ CO_2, (i) sample made at 102 °C and 3.5 mL min⁻¹ CO_2.

escape of CO_2. With decreasing temperature, the difference between E_T^M and E_T diminishes. The highest R_E calculated was 73% at 112 °C indicating that the full foaming potential of CO_2 has almost been reached. With further temperature diminution, a decrease in the ratio of expansion is observable. This is due to the increasing melt strength, preventing the CO_2 to give its maximum blowing effect.

To our knowledge, only few studies have investigated the type of expansion at the die exit[29,49] and none of them with PLA. The radial and longitudinal expansions are plotted as a function of temperature in Figure 8. Like Naguib et al.[29] have observed with polypropylene, the lower the temperature, the higher the radial expansion because of less gas loss. Here, the maximum radial expansion is about 6, representing an extrudate diameter of 18.5 mm. But with a further decrease in temperature, under 107 °C, the radial expansion begins to decrease. Now by comparing to the longitudinal expansion on Figure 8(b), it appears that with the die temperature diminution, the longitudinal expansion decreases slightly. This is linked to an increase in

diameter. But, below the temperature of 110 °C, the longitudinal expansion increased to finally reach the value of 2.4 at 102 °C (representing a speed of 7 m min⁻¹). This clearly indicates a change of phenomenology. Due to the increasing polymer stiffness at low temperature, leading to a "frozen" surface of the extrudate, the gas can no longer escape from this surface. In consequence, the gas will push the sample out of the die axially, increasing the longitudinal expansion.

In terms of mass balance, the average difference between the measured and calculated mass flow for all samples is ±25%. This relative high value can be explained by the irregular shape of the samples giving a large degree of imprecision in eq. (9) but confirm our results on the change of phenomenology between the radial and longitudinal expansions.

Structure of the Foams

Figure 9 shows the morphology of the foams. For Figure 9(a,b), at high die temperature, foam structure is really coarse with only few big cells. But, with the diminution of temperature, cell

density increased while cell size diminishes as seen on Figure 9(c f). The morphology remains coarse with broken and opened cell walls. These pictures [Figure (a f)] are in good correlation with the open porosity content seen in Figure 3. Indeed, the porosity presented at these temperatures is only open porosity.

Conversely, Figure 9(g i) shows a closed cell morphology, with a lot of small cells. This is again consistent with the porosity presented in Figure 3, almost all porosity created being closed.

Differences between Figure 9(a c) and the other images illustrate the competition between nucleation and growth. Park *et al.* have shown that, due to competition between nucleation and diffusion, a higher pressure drop rate will result in higher supersaturation, which translates to a higher nucleation rate.[50] It can be seen in Figure 6 that the pressure between 110 and 130 °C is pretty constant (9 MPa) and leads to low cell density [Figure 9(a c)] with high cell size. But below 110 °C, the die pressure increases (between 10 and 16 MPa) because of the increased viscosity, and this leads in turn to a higher cell density [Figure 9(d i)] but at the expense of the growth. Indeed, the cells could not grow due to stiff cell walls.[20] Particularly, for the foam samples made at 103 °C and 3.5 mL min^{-1} flow CO_2, die pressure was about 14 MPa and the SEM images show high cell density with low cell size.

CONCLUSIONS

The process of extrusion foaming of PLA with supercritical CO_2 and the importance of operating conditions on foam properties have been investigated. The influence of the temperature before and in the die has been demonstrated.

At the highest die temperatures, the effect of shear was not predominant, hence almost no crystallinity was induced, resulting in poor melt strength. Therefore, a large radial expansion of the foams was obtained and large extrudate with a diameter up to 18 mm could be obtained. These foams with such a high radial expansion exhibited an open porosity structure, with total porosity as high as 96%. The pressure upstream the die was about 9 MPa. At lower die temperatures, the crystallinity of the sample increased resulting in a higher melt strength. Due to the relative low die temperature, the surface extrudate was "frozen," and hence the radial expansion was replaced by longitudinal expansion. In this case, the foams present closed cell morphology because the CO_2 cannot escape from the cell walls. However, the total porosity remains high (>92%).

Competition between cell nucleation and growth was observed. Increased crystallinity is coupled with higher pressure. As a consequence, the foams with high crystallinity present a lot of cells with a small size while at the opposite, the foams with low crystallinity presented less cells of bigger size.

Depending on the operating parameters, two different kinds of foam: (i) high porosity, with large extrudate diameter and only open cell or (ii) high porosity, with a small extrudate diameter with a lot of closed cell, have been created. These two types of foam could be used in different applications. For instance, open porosity foams might be used in scaffolds applications whereas closed porosity foams could be used in packaging or cushioning applications. Nevertheless, both types of applications could benefit from the inherent properties of the poly(lactic acid): it is a biobased, biodegradable, and biocompatible polymer.

REFERENCES

1. Auras, R.; Harte, B.; Selke, S. *Macromol. Biosci.* **2004**, *4*, 835.

2. Nofar, M.; Park, C. B. *Prog. Polym. Sci.* **2014**, *39*, 1721.

3. Glenn, G. M.; Orts, W. *J. Ind. Crops Prod.* **2001**, *13*, 135.

4. Nair, L. S.; Laurencin, C. T. *Prog. Polym. Sci.* **2007**, *32*, 762.

5. Jing, X.; Mi, H.; Cordie, T.; Salick, M.; Peng, X.; Turng, L. *Ind. Eng. Chem. Res.* **2015**, *53*, 17909.

6. Zhao, H.; Cui, Z.; Sun, X.; Turng, L. S.; Peng, X. *Ind. Eng. Chem. Res.* **2013**, *52*, 2569.

7. Liu, B.; Jiang, L.; Zhang, J. *Macromol. Mater. Eng.* **2011**, *296*, 835.

8. Zhang, J.; Rizvi, G. M.; Park, C. B.; Hasan, M. M. *J. Mater. Sci.* **2011**, *46*, 3777.

9. Sauceau, M.; Fages, J.; Common, A.; Nikitine, C.; Rodier, E. *Prog. Polym. Sci.* **2011**, *36*, 749.

10. Reigner, J.; Gendron, R.; Champagne, M. F. *Cell. Polym.* **2007**, *26*, 83.

11. Mihai, M.; Huneault, M. A.; Favis, B. D.; Li, H. *Macromol. Biosci.* **2007**, *7*, 907.

12. Mihai, M.; Huneault, M. A.; Favis, B. D. *J. Appl. Polym. Sci.* **2009**, *113*, 2920.

13. Larsen, Å.; Neldin, C. *Polym. Eng. Sci.* **2013**, *53*, 941.

14. Pilla, S.; Kim, S. G.; Auer, G. K.; Gong, S.; Park, C. B. *Polym. Eng. Sci.* **2009**, *49*, 1653.

15. Mihai, M.; Huneault, M. A.; Favis, B. D. *Polym. Eng. Sci.* **2010**, *50*, 629.

16. Wang, J.; Zhu, W.; Zhang, H.; Park, C. B. *Chem. Eng. Sci.* **2012**, *75*, 390.

17. Keshtkar, M.; Nofar, M.; Park, C. B.; Carreau, P. J. *Polymer (Guildford)* **2014**, *55*, 4077.

18. Matuana, L. M.; Diaz, C. A. *Ind. Eng. Chem. Res.* **2010**, *49*, 2186.

19. Jiang, G.; Huang, H. X.; Chen, Z. K. *Adv. Polym. Technol.* **2011**, *30*, 174.

20. Pilla, S.; Kim, S. G.; Auer, G. K.; Gong, S.; Park, C. B. *Mater. Sci. Eng. C* **2010**, *30*, 255.

21. Matuana, L. M.; Diaz, C. A. *Ind. Eng. Chem. Res.* **2013**, *52*, 12032.

22. Nofar, M. *Mater. Des.* **2016**, *101*, 24.

23. Bocz, K.; Tábi, T.; Vadas, D.; Sauceau, M.; Fages, J.; Marosi, G. *eXPRESS Polym. Lett.* **2016**, *10*, 771.

24. Chauvet, M.; Sauceau, M.; Fages, J. *J. Supercrit. Fluids* **2017**, *120*, 408.

25. Jeon, B.; Kim, H. K.; Cha, S. W.; Lee, S. J.; Han, M. S.; Lee, K. S. *Int. J. Precis. Eng. Manuf.* **2013**, *14*, 679.

26. Park, C. B.; Padareva, V.; Lee, P. C.; Naguib, H. E. *J. Polym. Eng.* **2005**, *25*, 239.

27. Lee, J. W. S.; Wang, K.; Park, C. B. *Ind. Eng. Chem. Res.* **2005**, *44*, 92.

28. Huang, Q.; Seibig, B.; Paul, D. *J. Membr. Sci.* **1999**, *161*, 287.

29. Naguib, H. E.; Park, C. B.; Reichelt, N. *J. Appl. Polym. Sci.* **2004**, *91*, 2661.

30. Nikitine, C.; Rodier, E.; Sauceau, M.; Letourneau, J.; Fages, J. *J. Appl. Polym. Sci.* **2010**, *115*, 981.

31. Nikitine, C.; Rodier, E.; Sauceau, M.; Fages, J. *Chem. Eng. Res. Des.* **2009**, *87*, 809.

32. Le Moigne, N.; Sauceau, M.; Benyakhlef, M.; Jemai, R.; Benezet, J. C.; Rodier, E.; Lopez Cuesta, J. M.; Fages, J. *Eur. Polym. J.* **2014**, *61*, 157.

33. Nagy, Z. K.; Sauceau, M.; Nyúl, K.; Rodier, E.; Vajna, B.; Marosi, G.; Fages, J. *Polym. Adv. Technol.* **2012**, *23*, 909.

34. Carbon dioxide, NIST Chemistry WebBook. Available at: http://webbook.nist.gov/cgi/cbook.cgi?ID=124 38 9.

35. Span, R.; Wagner, W. *J. Phys. Chem. Ref. Data* **1996**, *25*, 1509.

36. Fischer, E. W.; Sterzel, H. J.; Wegner, G. *Colloid Polym. Sci.* **1973**, *251*, 980.

37. Park, C. B.; Behravesh, A. H.; Venter, R. D. *Polym. Eng. Sci.* **1998**, *38*, 1812.

38. Rauwendaal, C. Polymer Extrusion, 4th ed.; Hanser Publishers, Munich, **2001**; Chapter 7, p 210.

39. Behravesh, A.; Park, C.; Pan, M.; Venter, R. *12th Natl. ACS Meet. Polym. Prepr.* **1996**, *37*, 767.

40. Naguib, H. E.; Park, C. B.; Lee, P. C. *J. Cell. Plast.* **2003**, *39*, 499.

41. Cai, H.; Dave, V.; Gross, R. A.; McCarthy, S. P. *J. Polym. Sci. Part B: Polym. Phys.* **1996**, *34*, 2701.

42. Lim, L. T.; Auras, R.; Rubino, M. *Prog. Polym. Sci.* **2008**, *33*, 820.

43. Yasuniwa, M.; Tsubakihara, S.; Sugimoto, Y.; Nakafuku, C. *J. Polym. Sci. Part B: Polym. Phys.* **2004**, *42*, 25.

44. Nofar, M.; Ameli, A.; Park, C. B. *Macromol. Mater. Eng.* **2014**, *299*, 1232.

45. Tsutsumi, C.; Watanabe, R.; Tokumaru, A.; Kuwaoka, N.; Nakayama, Y.; Shiono, T. *J. Appl. Polym. Sci.* **2016**, *133*, DOI: 10.1002/app.44006.

46. Nofar, M.; Tabatabaei, A.; Ameli, A.; Park, C. B. *Polymer (Guildford)* **2013**, *54*, 6471.

47. Vleeshouwers, S.; Meijer, H. E. H. *Rheol. Acta* **1996**, *35*, 391.

48. Sawai, D.; Takahashi, K.; Imamura, T.; Nakamura, K.; Kanamoto, T.; Hyon, S. H. *J. Polym. Sci. Part B: Polym. Phys.* **2002**, *40*, 95.

49. Spitael, P.; Macosko, C. W. *Polym. Eng. Sci.* **2004**, *44*, 2090.

50. Park, C. B.; Baldwin, D. F.; Suh, N. P. *Polym. Eng. Sci.* **1995**, *35*, 432.